LAWRENCE
LIVERMORE
NATIONAL
LABORATORY

LLNL-JRNL-635901

Deflection of MeV electrons by self-generated magnetic fields in intense laser-solid interaction

F. Perez, A. J. Kemp, L. Divol, C. D. Chen, P. K. Patel

April 30, 2013

Physical Review Letters

Disclaimer

This document was prepared as an account of work sponsored by an agency of the United States government. Neither the United States government nor Lawrence Livermore National Security, LLC, nor any of their employees makes any warranty, expressed or implied, or assumes any legal liability or responsibility for the accuracy, completeness, or usefulness of any information, apparatus, product, or process disclosed, or represents that its use would not infringe privately owned rights. Reference herein to any specific commercial product, process, or service by trade name, trademark, manufacturer, or otherwise does not necessarily constitute or imply its endorsement, recommendation, or favoring by the United States government or Lawrence Livermore National Security, LLC. The views and opinions of authors expressed herein do not necessarily state or reflect those of the United States government or Lawrence Livermore National Security, LLC, and shall not be used for advertising or product endorsement purposes.

Deflection of MeV electrons by self-generated magnetic fields in intense laser-solid interaction

F. Pérez,* A. J. Kemp, L. Divol, C. D. Chen, and P. K. Patel
Lawrence Livermore National Laboratory, Livermore, California 94550, USA

Relativistic electrons generated in the interaction of intense picosecond laser pulses with solid targets can be deflected by strong self-generated magnetic fields near the target surface, considerably turning their average direction away from the laser axis. This effect has significance for the interpretation of laser experiments, in particular for the characterization of the laser-accelerated electron beams in applications such as laser-driven ion acceleration or the fast-ignition scheme for inertial confinement fusion.

Intense-laser interaction with dense plasmas finds multiple applications in modern physics. In particular, laser-accelerated suprathermal electrons play an important role in warm-dense-matter studies [1], ion acceleration [2], and in fast-ignition inertial confinement fusion [3]. In the past twenty years, their spectrum [4], amount [5], and angular distribution [6] were investigated, as well as how they relate to laser or target parameters [7]. In this Letter, we show that the fast-electron angular distribution, in fairly common laser configurations, can be strongly affected by magnetostatic fields induced by the reflected light.

Previous studies reported fast-electron beams oriented along the laser axis or closer to the target normal [8–10]. In the present study, the strong (10^4 T) magnetic fields in the underdense pre-plasma preceding the solid target turn energetic electrons away from their initial average direction − the laser axis. Multiple-MeV electrons are consistently deflected, as illustrated in Fig. 1. This effect is not described in previous literature which often featured either normal or large (45°) incidence. Our study uses a 16° incidence angle, common in laser-plasma interaction (LPI) experiments. Under this condition, the incident and reflected laser beams significantly overlap, which we show to be responsible for the electron deflection. The main cause for this effect are magnetostatic fields in the pre-plasma. They are known to be generated during the LPI [11], but the dominant magnetic fields in our study are induced by the reflected laser light, which was not investigated before.

The signature of these fast electrons can only be found from indirect measurements such as x-ray line emission [12], Bremsstrahlung [5] or transition radiation [13]. Our finding is supported by recent experimental results using Bremsstrahlung detectors to characterize the electron spectrum in different directions. However, experimental data do not completely describe the angular distribution: to infer their average direction and divergence, complex modeling of the measured radiation is required, and multiple matching situations may be found. We detail here numerical simulation results to describe the physics of the observed electron deflection.

Three-dimensional simulations, carried out using the collisional explicit particle-in-cell (PIC) code *PSC* [14], featured a $20 \times 30 \times 42$ μm^2 box with 16 cells per micron and 16 particles of each species per cell, and contained an Al plasma slab of maximum density 100 n_c, where $n_c = \varepsilon_0 m_e (2\pi c)^2/(e\lambda)^2$ is the critical electron density at the laser wavelength $\lambda = 1$ μm. The envelope of the p-polarized laser field was gaussian with a 3 μm waist which focuses to $I = 2 \times 10^{19}$ W/cm^2 when in vacuum, with a 16° angle of incidence with respect to the target normal. Its intensity temporal shape was a 0.4 ps full-width-at-half-maximum (FWHM) gaussian starting at 2% of the maximum intensity, reaching peak power at 600 fs. The density and level of ionization of the plasma preceding the dense target resemble that from hydrodynamic simulations relevant to the pre-pulse energy of the Titan laser system at the Lawrence Livermore National Laboratory. The electron density profile is characterized by a double-exponential with scale-lengths of 1 and 15 μm, the critical density being displaced by 5 μm from the target surface. For simplicity, it was chosen transversely uniform,

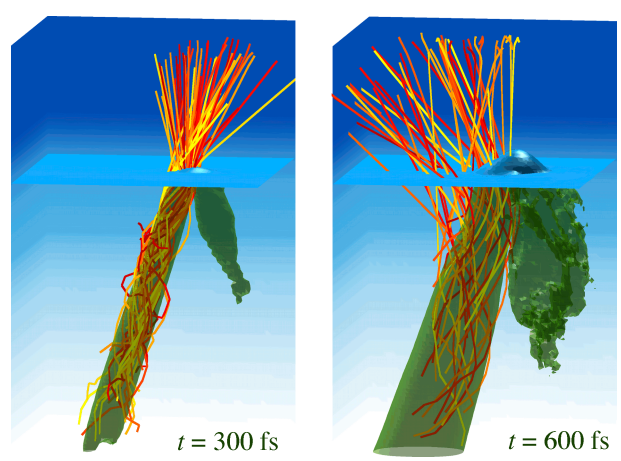

FIG. 1. (Color online) Electron deflection in 3D PIC simulation at quarter peak power (left) and at peak power (right). Incident and reflected laser envelopes as green isosurfaces (at intensities 2×10^{18} and 0.4×10^{18} W/cm^2, respectively), fast (> 5 MeV) electron trajectories in orange, and target density in blue, with a slice at the critical electron density. The plotted box size is $16 \times 16 \times 30$ μm^3.

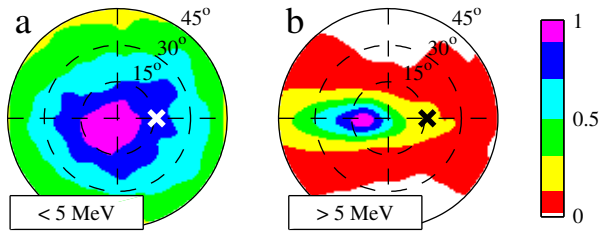

FIG. 2. (Color online) Time-integrated angular distributions of (a) the < 5 MeV electrons and (b) the > 5 MeV electrons that reach the dense plasma region. The laser direction is given by crosses and 0° is the target normal.

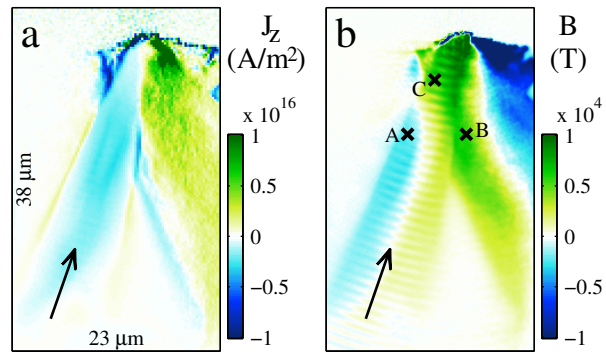

FIG. 3. (Color online) 3D PIC simulation results in the incidence plane, at peak power: (a) z-component of electron current density and (b) laser-cycle-averaged magnetic field. Arrows indicates the laser direction. The represented box size is given in the figure.

because no noticeable influence of the transverse profile was observed in corresponding 2D simulations. Similarly, collisions were not included after verifying that their role was minimal.

Previous experimental studies [8–10] have shown that electrons which acquire an energy above the laser ponderomotive energy (a few MeV) are directed, in average, along the laser axis, as they remain in the laser field for a long time, and are accelerated on a long distance. These studies were performed with a 45° incidence, which is known for significant laser refraction [15], thus with potentially different LPI. Instead, our simulations, using a 16°, slightly oblique incidence relevant to recent experiments on the Titan laser, show that multi-MeV electrons turn away from the laser axis. This deflection is illustrated in Fig. 1 showing electron trajectories turning with respect to the laser direction (macro-particle trajectories were randomly selected among the > 5 MeV electrons that reached the solid density region). At early times, electrons accelerated to more than 5 MeV are aligned with the laser direction ($\sim 16°$), but they are strongly deflected (up to $-40°$) after 400 fs. The time-integrated angular electron distribution (in both polar and azimuthal angles) is plotted in Fig. 2. Electrons below 5 MeV (Fig. 2a) are distributed evenly around the target normal. The distribution of > 5 MeV electrons (Fig. 2b) peaks at $-8°$ and extends to $-40°$. The corresponding divergence half-angle is $\sim 15°$ in the incidence plane, and $\sim 6°$ in the transverse direction. Note that this small transverse divergence is related to the laser polarization: we obtained a broader transverse divergence in a simulation with s-polarization (the electron deflection effect was still present). In total, 75% of these fast electrons turn further than the target normal, containing 25% of the total electron energy that entered the solid target.

The cause of this deflection are strong magnetostatic fields generated in the underdense pre-plasma preceding the solid target. The laser stochastically accelerates electrons [16] in the region from 0.01 n_c to 1 n_c (5 to 30 μm away from the solid target). Electrons directed along the laser axis are continuously accelerated, thus form a strong current aligned with the laser, as illustrated in Fig. 3a. The maximum possible current density along the laser path is $j \sim e\,c\,n_e \sim 5 \times 10^{15}$ A/m^2 with a typical electron density $n_e = 0.1\,n_c$. For a laser beam radius of $R = 5$ μm, this creates an azimuthal magnetic field $B = \mu_0 R\,j/2 \sim 10^4$ T surrounding the beam, clearly visible in Fig. 3b. It is strong enough to confine multi-MeV electrons inside its path. Example trajectories of such electrons, confined around the laser axis up to the solid target at early times, are plotted in Fig. 1.

At later times, the dominant contribution to the magnetic field is due to the reflected light. The laser reflection is close to specular, the path the reflected light being symmetrical to the incident one with respect to target normal. Figure 3a shows a stronger current in the path of specularly reflected light, which translates to a stronger magnetic field, as seen in Fig. 3b. Because the density gradient scale-length is sufficiently long (1 to 10 μm) at the LPI region, the reflected light is able to draw a strong current from this dense plasma. Our simulations indicate that 15% of the laser energy is reflected close to the specular direction. Due to scattering and re-absorption, the reflected laser intensity decreases over a few microns, but accelerates "specular" electrons in a large number. These electrons are accelerated to a lower average energy, ~ 1 MeV, because of the lower light intensity [17], but their velocity remains close to c. Hence, the static magnetic field they induce is stronger than the one due to the incident laser.

This asymmetry between incident and specular paths can be explained by the laser ponderomotive potential evacuating electrons sideways, thus creating a channel, as illustrated in Fig. 4a. The electron density on the laser path is decreased by a factor 10 at peak power. On the other hand, the intensity of the reflected light is too low to significantly reduce electron density. This density in the specular path is actually replenished by the plasma pushed away from the laser path. Figure 4b shows the

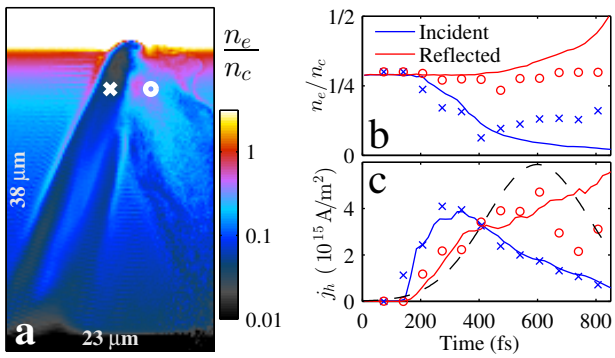

FIG. 4. (Color online) Channeling in the 3D PIC simulation at the incidence plane: (a) electron density map at peak power, (b) its time dependence at the points indicated in (a), and (c) the corresponding current. Circles and crosses in (b) and (c) are the models of Eqs. (1) and (2) with $\kappa = 3 \times 10^{-22}$ cm^3. Dashed black line: injected maximum laser intensity in arbitrary units.

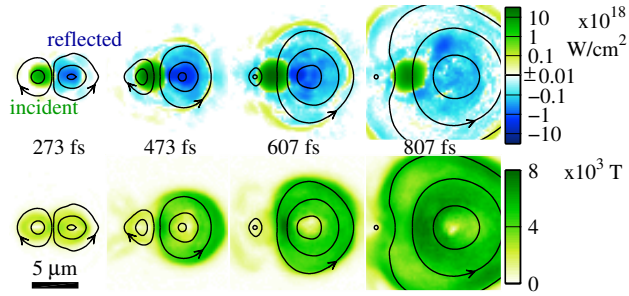

FIG. 5. (Color online) Maps from the 3D PIC simulation in a plane parallel to the solid surface (5 μm away). Top row: Poynting flux. Bottom row: magnetic field magnitude. Black lines illustrate a few magnetic field lines.

time-dependence of the electron density n_e inside both the laser path and the specular path (5 μm away from the target surface). We compared this channeling to a known model [18] which, for a gaussian beam with the intensity envelope $\exp(-r^2/R^2)$, predicts a density variation

$$\frac{\delta n_e}{n_c} = \left(\frac{\lambda}{2\pi R}\right)^2 \frac{a_0^2/2}{\sqrt{1+a_0^2/2}} \tag{1}$$

where $a_0^2 = I\lambda^2 \times \mu_0 e^2/\left(\pi^2 m_e^2 c^3\right)$. The model is illustrated with markers on Fig. 4b. Even though Eq. (1) neglects ion motion, which starts to play a role after 500 fs, and the interaction between the incident and specular channels, the good agreement with the simulation results shows that channeling is significant.

Figure 4c demonstrates how this change in density affects the currents (solid lines). Before 300 fs, the incident current is 1 to 5 times higher than the specular one. Later, the incident current decreases, matching the density decrease in the channel. On the contrary, no significant channel is formed by the specular light, thus the specular current does not decrease. As a consequence, the specular current overcomes the incident one after 400 fs.

We have developed a model that reproduces the evolution of these currents due to the variation of the electron density and of the laser intensity. The relativistic electron current density is $j_h \simeq e\,c\,n_h$, where n_h is their density. The hot-electron ponderomotive energy from Ref. [17] can be approximated to $T_h \simeq m_e c^2 a_0$ for $a_0 \gg 1$ (note that other studies obtain similar scaling in $\sqrt{I}$, see Ref. [16, 19]). Given a laser-to-hot-electron conversion efficiency η, the fast-electron energy flux density $c n_h T_h$ is equal to ηI. Furthermore, assuming that electrons are accelerated independently of each other, the conversion efficiency η is proportional to the background electron density n_e, i.e. $\eta = \kappa n_e$, where we use κ as a fitting parameter. Overall, this model leads to a fast-electron current

$$j_h = \frac{e\,c\,n_c}{2\sqrt{2}}\,\kappa\,n_e\,a_0. \tag{2}$$

Figure 4c shows that the current (solid lines) is reproduced very satisfyingly by this formula (markers) where intensity and background density vary with time. This confirms that channeling is the key effect responsible for the asymmetry of currents.

The current asymmetry is also caused by the reflected light being spread out at later times. Figure 5 (top row) shows snapshots of the laser Poynting flux in a plane parallel to the target, 5 μm away from the solid surface. The incident laser spot (top, in green) barely changes in size, while the reflected light (top, blue area) evolves from a fairly collimated beam to a wide emission. This widening is likely due to deformation and rippling of the reflecting surface at critical density, also observed in the simulations. The current consequently broadens from a thin beam to a wide cone, which causes the magnetic field from the reflected light to further overcome the incident one, as shown in Fig. 5 (bottom row).

Figure (6) demonstrates that the magnitude of the magnetic field in he pre-plasma can be estimated from simple magnetostatics calculations. The laser-cycle-averaged fields and currents from the 3D PIC simulation are related through Ampère's law $\nabla \times \langle \mathbf{B} \rangle = \mu_0 \langle \boldsymbol{j} \rangle$, the displacement current being insignificant beyond the laser period time-scale. Modeling the incident and specular currents as two superimposed infinite cylinders of different current densities, we calculated the magnetic fields on points A, B and C defined on Fig. 3b (fields, currents and cylinder radii were measured *vs* time in the 3D PIC simulation). Points A and B illustrate the incident and specular contributions, respectively. Point C is representative of the location where fast electrons are deflected, and where magnetic fields are a combination of both incident and specular beams. Figure 6 shows that the magnetostatic model matches well the actual fields.

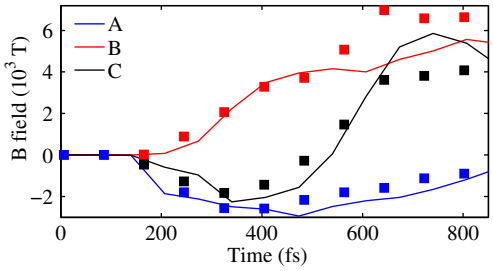

FIG. 6. (Color online) 3D PIC simulation magnetic field *vs* time, at points A, B and C from Fig. 3b. Squares illustrate the simple magnetostatics calculation explained in the text.

The field at point C matches the contribution from the incident laser (at point A) until 400 fs, and later matches the contribution from the specular light (at point B) because the specular current gradually overcomes the incident one.

As a consequence to this magnetic field evolution, fast electrons traveling within the laser path experience, after peak power. a magnetic field that deflects them away from their initial direction. This explains our observation of an electron beam directed away from the laser axis.

Electrons with smaller energies, between 0.1 and 5 MeV, do not exhibit this turning, and are instead directed in average about the target normal. Their trajectories revealed two kinds of behavior. First, they may originate from the dense region and briefly get to the LPI area where they are accelerated back in the target. Local fields scatter them widely so there is no influence of the laser direction. Second, electrons may gyrate for a while due to the static magnetic fields, eventually reaching the target surface and entering the target with a wide angular distribution. In fact, electrons must have a Larmor radius larger than the lateral extent of the magnetic fields (~ 5 μm) to enter the solid target: this corresponds, in our situation, to an energy > 5 MeV.

Recent experimental data, subject of a separate publication by C. D. Chen *et al*, were found consistent with the electron deflection effect. The Titan laser was incident at 16° on a flat 10 μm Al foil backed with a thick Ag slab. Bremsstrahlung emission was collected into detectors at different angles around the target. Comparing with electron transport and Bremsstrahlung detection simulations, best agreement was found when the high-energy electron component matched the turning effect described above. When it was set in other directions, such as the target normal or the laser axis, or was even artificially removed, the agreement was not as good.

The mechanism described here requires the specular beam to overlap significantly with the incident one and the reflected light to be intense enough to accelerate strong currents. We thus expect that larger incidence angles and less intense lasers do not show turning electrons. This is consistent with previous experimental results [8–10] which used an incidence angle of 45° and an intensity of $\sim 10^{19}$ W/cm^2. Note that such a large angle of incidence also induces significant refraction: the laser path is bent and may not reach high-enough densities to create strong currents.

In conclusion, we observe a significant deflection of multi-MeV electrons accelerated by an intense laser obliquely incident on a solid target. 3D PIC simulations show that these electrons originate in the underdense pre-plasma where they are accelerated and confined in the laser path by their self-generated magnetic field. After peak power, they are deflected by the magnetostatic field originating from reflected-light-accelerated electrons. This effect is best seen in configurations with non-grazing incidence, significant pre-plasma, channeling and reflected light, which are all fairly common characteristics of picosecond-laser interaction experiments.

Simulations were carried out on the Livermore Computing Center's Sierra cluster under a LLNL Grand Challenge allocation. This work was performed under the auspices of the U.S. Department of Energy by the Lawrence Livermore National Laboratory under Contract No. XXXX.

Prepared by LLNL under Contract DE-AC52-07NA27344.

* perez75@llnl.gov

[1] P. M. Nilson, *et al.*, Phys. Rev. E **79**, 016406 (2009); A. Mančić, *et al.*, Phys. Rev. Lett. **104**, 035002 (2010); Y. Ping, *et al.*, High Energy Density Phys. **6**, 246 (2010).
[2] M. Borghesi, *et al.*, Fusion Sci. Technol. **49**, 412 (2006); J. Badziak, Opto-Electron. Rev. **15**, 1 (2007); H. Daido, M. Nishiuchi, and A. S. Pirozhkov, Rep. Prog. Phys. **75**, 056401 (2012).
[3] M. Tabak, *et al.*, Phys. Plasmas **1**, 1626 (1994).
[4] H. Sawada, *et al.*, Phys. Plasmas **19**, 103108 (2012).
[5] C. D. Chen, *et al.*, Phys. Plasmas **16**, 082705 (2009).
[6] A. Debayle, J. Honrubia, E. d'Humières, and V. Tikhonchuk, Phys. Rev. E **82**, 036405 (2010).
[7] J. S. Green, *et al.*, Phys. Rev. Lett. **100**, 015003 (2008); S. Chawla, *et al.*, Phys. Rev. Lett. **110**, 025001 (2013).
[8] P. A. Norreys, *et al.*, Phys. Plasmas **6**, 2150 (1999).
[9] M. I. K. Santala, *et al.*, Phys. Rev. Lett. **84**, 1459 (2000).
[10] B. I. Cho, *et al.*, Phys. Rev. E **80**, 055402 (2009).
[11] J. A. Stamper, *et al.*, Phys. Rev. Lett. **26**, 1012 (1971); M. G. Haines, Can. J. Phys. **64**, 912 (1986); A. Pukhov and J. Meyer-ter Vehn, Phys. Rev. Lett. **76**, 3975 (1996); M. Tatarakis, *et al.*, Phys. Plasmas **9**, 2244 (2002).
[12] R. B. Stephens, *et al.*, Phys. Rev. E **69**, 066414 (2004).
[13] J. J. Santos, *et al.*, Phys. Rev. Lett. **89**, 025001 (2002).
[14] A. J. Kemp, B. I. Cohen, and L. Divol, Phys. Plasmas **17**, 056702 (2010).
[15] R. H. H. Scott, *et al.*, Phys. Plasmas **19**, 053104 (2012).
[16] J. T. Mendonça and F. Doveil, J. Plasma Phys. **28**, 485 (1982); A. Pukhov, Z.-M. Sheng, and J. Meyer-ter Vehn, Phys. Plasmas **6**, 2847 (1999); A. J. Kemp, Y. Sentoku, and M. Tabak, Phys. Rev. E **79**, 066406 (2009).
[17] S. C. Wilks, W. L. Kruer, M. Tabak, and A. B. Langdon, Phys. Rev. Lett. **69**, 1383 (1992).

[18] E. Esarey, P. Sprangle, J. Krall, and A. Ting, IEEE T. Plasma Sci. **24**, 252 (1996).

[19] H. Xu, Z.-M. Sheng, J. Zhang, and X.-T. He, Phys. Scripta **77**, 045502 (2008).